Journal of Hazardous Materials 175 (2010) 429–438

Contents lists available at ScienceDirect

Journal of Hazardous Materials

journal homepage: www.elsevier.com/locate/jhazmat

Mixed phase titania nanocomposite codoped with metallic silver and vanadium oxide: New efficient photocatalyst for dye degradation

Xia Yang[a,b], Fengyan Ma[b], Kexin Li[b], Yingna Guo[b], Jianglei Hu[b], Wei Li[b], Mingxin Huo[a,*], Yihang Guo[b,*]

[a] School of Urban and Environmental Sciences, Northeast Normal University, Changchun 130024, PR China
[b] School of Chemistry, Northeast Normal University, Changchun 130024, PR China

ARTICLE INFO

Article history:
Received 21 August 2009
Received in revised form 4 October 2009
Accepted 5 October 2009
Available online 13 October 2009

Keywords:
Silver
Vanadium oxide
Titania
Nanocomposite
Dye
Photocatalysis

ABSTRACT

Titania nanocomposite codoped with metallic silver and vanadium oxide was prepared by a one-step sol–gel–solvothermal method in the presence of a triblock copolymer surfactant (P123). The resulting Ag/V–TiO_2 three-component junction system exhibited an anatase/rutile (weight ratio of 73.8:26.2) mixed phase structure, narrower band gap (2.25 eV), and extremely small particle sizes (ca. 12 nm) with metallic Ag particles well distributed on the surface of the composite. The Ag/V–TiO_2 nanocomposite was used as the visible- and UV-light-driven photocatalyst to degrade dyes rhodamine B (RB) and coomassie brilliant blue G-250 (CBB) in an aqueous solution. At 1.8% Ag and 4.9% V doping, the Ag/V–TiO_2 system exhibited the highest visible- as well as UV-light photocatalytic activity; additionally, the activity of the three-component system exceeded that of Degussa P25, pure TiO_2, single-doped TiO_2 system (Ag/TiO_2 or V–TiO_2) as well as P123-free-Ag/V–TiO_2 codoped system. The reasons for this enhanced photocatalytic activity were revealed.

1. Introduction

Dyes are natural and xenobiotic compounds that make the world more beautiful through coloured substances. However, the release of coloured wastewaters represents a serious environmental problem and a public health concern. Colour removal, especially from textile wastewaters, has been a big challenge over the last decades, and up to date there is no single and economically attractive treatment that can effectively decolourise dyes [1]. Photocatalytic degradation of various types of dyes in water by UV-light irradiated TiO_2 is considered as a valuable technique for purifying and reusing aqueous effluents [2–4]. However, two main drawbacks including low quantum efficiency due to the high recombination rate of photoinduced electron–hole pairs (e^-–h^+) and poor absorption ability in the visible-light region limit the efficiency of TiO_2 photocatalytic reactions. Therefore many efforts have been devoted to extend the spectral response of TiO_2 into the visible-light region and improve the quantum efficiency of TiO_2, which have profound positive effect on the efficient use of solar energy in photocatalytic reactions.

Common approaches to develop TiO_2-based visible-light-driven photocatalysts include: (i) substitution of Ti by transition metal [5,6]; (ii) doping with nonmetal atoms [7,8] or other semiconductors [9]; (iii) reducing the size of TiO_2; (iv) changing the morphology and phase structure and composition of TiO_2; and (v) adding hole scavengers [10]. More recently, an noble metal (*e.g.*, Au, Ag, Pt, Pd, or Rh) and a small band gap semiconductor (*e.g.*, CdS, In_2O_3, Fe_2O_3, or $InVO_4$) codoped TiO_2 three-component junction systems have attracted considerable interest since these junction systems can result in higher photocatalytic activity and peculiar characteristics in comparison with pure TiO_2 or two-component junction systems (*i.e.*, noble metal/TiO_2 or semiconductor/TiO_2 systems). This enhanced photocatalytic activity originated from the co-operation of the electron trapping ability of noble metal and decreased band gap energy owing to doping a small band gap semiconductor. For examples, Pt and CdS codoped TiO_2 system CdS/(Pt/TiO_2) showed the highest rate of hydrogen production under visible-light irradiation in comparison with CdS/TiO_2 or Pt/CdS single component doped system [11]; Ag and $InVO_4$ codoped TiO_2 composite thin film with 1% Ag doping exhibited higher visible-light photocatalytic activity for decomposition of aqueous methyl orange compared with TiO_2 or $InVO_4$–TiO_2 [12].

Motivated by the above successful applications our current work focuses on the preparation of nanoscale metal Ag and vanadium oxide codoped TiO_2 three-component junction system. It is reported that vanadium ion had the highest effectiveness in the red shift of the spectral response of TiO_2 [13]. Vanadium oxide doped TiO_2 seems one of the best alternatives to extend the optical absorption of TiO_2 towards the visible-light region [14]. The researchers attributed this enhanced photocatalytic activity of V–TiO_2 two-component junction system to the following one or several reasons:

* Corresponding authors. Tel.: +86 431 85098705; fax: +86 431 85098705.
E-mail address: guoyh@nenu.edu.cn (Y. Guo).

0304-3894/$ – see front matter © 2009 Elsevier B.V. All rights reserved.
doi:10.1016/j.jhazmat.2009.10.024

(i) the enhanced absorption in the visible-light region; (ii) the improved quantum efficiency owing to improve the e^-–h^+ pair separation efficiency; and/or (iii) the presence of both V^{4+} and V^{5+} species in the V-doped TiO_2 materials. V^{4+} can act as a trapping center for both h^+ and e^-, favoring charge separation, while V^{5+} might act as an electron acceptor [15–17]. As for metal silver, it is particularly suitable for industrial applications due to its low cost and easy preparation. In the photocatalytic applications, silver nanoparticles deposited on the TiO_2 surface have been reported to increase the efficiency of the photocatalytic process by acting as electron sinks and thereby decreasing the recombination rate of e^-–h^+ pairs [18,19]. Additionally, the surface plasmon resonance of silver nanoparticles may assist in the separation of e^-–h^+ pairs created in the TiO_2, which could also contribute to the enhanced photocatalytic activity [19]. So far, though V-doped TiO_2 and Ag-doped TiO_2 two-component junction systems have already shown efficient visible-light photocatalytic activities, few reports are published on metallic silver and vanadium oxide codoped TiO_2 photocatalysts. We expect that metallic silver and vanadium oxide codoped TiO_2 material may demonstrate a new and efficient three-component junction photocatalytic system.

Herein, metallic silver and vanadium oxide codoped titania nanocomposite (Ag/V–TiO_2) with high dispersion of silver particles deposited on the surface of the composite were prepared by a one-step sol–gel–solvothermal method in the presence of a triblock copolymer surfactant ($EO_{20}PO_{70}EO_{20}$, Pluronic P123). Generally, P123 is used as a good soft template to prepare ordered mesostructured materials [10], while in current work, P123 is expected to act as a dispersion agent to prevent Ag/V–TiO_2 particles from aggregation. The aim can be realized by designing the suitable preparation route. This good dispersion or reduced aggregation among Ag/V–TiO_2 particles is expected to increase the active site-reactant contact opportunity and facilitate the electron transport, accordingly, the quantum efficiency of the Ag/V–TiO_2 will be increased. The physicochemical properties of the resulting Ag/V–TiO_2 nanocomposites were characterized by X-ray photoelectron spectroscopy (XPS), X-ray diffraction (XRD), UV–vis diffuse reflectance spectra (UV–vis/DRS), transmission electron microscope (TEM), and nitrogen gas porosimetry. Subsequently, their UV- and visible-light photocatalytic activity was evaluated by the degradation of dyes RB and CBB, and the factors influencing the photocatalytic activity including phase structure and composition, Ag or V loadings, and adsorption behaviors of dyes were also investigated. For comparison, commercial TiO_2 (Degussa P25), as-prepared pure TiO_2, single-doped system (Ag/TiO_2 or V–TiO_2), and Ag/V–TiO_2 three-component junction system prepared in the absence of P123 were also examined under the identical reaction conditions.

2. Experimental

2.1. Catalyst preparation

P123 (2 g) was dissolved in isopropanol (i-PrOH, 10 mL) under vigorously stirring, and then ice-cooled titanium isoporpoxide (TTIP, 2 mL) was added, followed by further stirring for 30 min (mixture A). The other mixture of $AgNO_3$, NH_4VO_3, and 2 M HNO_3 (2.5 mL) (mixture B) was then added dropwise into mixture A under vigorously stirring, and the resulting mixture was continuously stirred until the gel was formed. The gel was transferred into an autoclave, heated to 473 K with a heating rate of 2 K min^{-1}, and then held at this temperature for 2 h. The compact gel was suffered from the following thermal treatment in vacuum: 313 K for 24 h, 333 K for 12 h, 353 K for 2 h, 373 K for 2 h, and 393 K for 0.5 h. Finally, the product was calcined at 723 K for 3 h. Ag/TiO_2, V–TiO_2, and pure TiO_2 were prepared similarly. For comparison, P123-free-Ag/V–TiO_2 samples were also obtained by the similar process in the absence of P123. The samples were denoted as Ag/V–TiO_2-(x, y), where x and y represent the determined doping level of Ag and V (wt%) in the products, respectively.

2.2. Catalyst characterization

The doping levels of Ag and V in the products were determined by a Leeman Prodigy Spec ICP-AES. UV–vis/DRS were recorded on a Cary 500 UV–vis–NIR spectrophotometer. XRD patterns were recorded on a Rigaku D/max-3c X-ray diffractometer (Cu Kα radiation, λ = 0.15405 nm), with α-silicon (99.999%) as a standard for the instrumental line broading. The crystallite size was calculated from the anatase (1 0 1) and the rutile (1 1 0) reflections located at 25.3° and 27.4°, respectively, by using the Debye–Scherrer equation [20]: $d = k\lambda/(\beta \cos\theta)$, where d is the crystallite size, k a constant of 0.9, λ the X-ray wavelength of Cu which is 0.15405 nm, θ the Bragg's angle in degrees, and β the full width at half maximum (FWHM) of the peak. The mass fraction of anatase (X_A) in the crystal lattice can be calculated based on the relationship between the integrated intensities of anatase (1 0 1) and rutile (1 1 0) peaks by the following formula developed by Spurr and Myers [21]: $X_A\ (\%) = 100/(1 + 1.265 I_R/I_A)$, where I_A and I_R are the integrated peak intensities of the anatase and rutile peak, respectively. In order to study the effects of doping on TiO_2 lattice, the lattice parameters of the powders were measured. For the anatase crystal system the lattice constants 'a' and 'c' were determined from two appropriate reflections ($h\,k\,l$) using the following formula [20]: $1/d^2 = (h^2 + k^2)/a^2 + l^2/c^2$. The value of d, for an XRD peak can be determined from the 2θ by Bragg's Law [20]: $d = \lambda/(2 \sin\theta)$, where λ is the X-ray wavelength which equals to 0.15405 nm for Cu Kα radiation and θ is the diffraction angle of the crystal plane ($h\,k\,l$). For this analysis, the peak positions (2θ) of the anatase (1 0 1) and (2 0 0) reflections were used to calculate the lattice parameters. XPS was performed on a VG-ADES 400 instrument with Mg Kα-ADES source at a residual gas pressure of below 10^{-8} Pa. All the binding energies were referenced to the C 1s peak at 284.6 eV of the surface adventitious carbon. TEM micrographs were obtained on a JEOL JEM-2010 transmission electron microscope at an accelerating voltage of 200 kV. Nitrogen porosimetry was performed on a Micromeritics ASAP 2010 instrument. Surface areas were calculated by using the BET equation. Pore size distributions were estimated from BJH desorption determination.

2.3. Photocatalytic test

2.3.1. Degradation of dyes under visible-light irradiation

The photoreactor was designed with an internal light source (a 400 W Xenon lamp with a main emission wavelength of 420 nm and an average light intensity of 3.2 mW cm^{-2}) surrounded by a water-cooling jacket (glass) to cool the lamp. The suspension containing the solid catalyst (0.3 g) and an aqueous solution of RB or CBB (25 mg L^{-1}, 100 mL) surrounded the light source. The suspension was ultrasonicated for 10 min and then stirred in the dark for 30 min to obtain a good dispersion and thus adsorption–desorption equilibrium between RB or CBB molecules and the catalyst surface was established. Subsequently, Xenon lamp was inserted into the suspension after its intensity became stable. The suspension was vigorously stirred during the light irradiation process (240 min). The acidity of the suspension was neutral, and the system was open to air. At given intervals of illumination, fixed amounts of reaction solution were taken out, centrifuged and filtrated, and the filtrates were analyzed. Decreases of the concentrations of RB or CBB were analyzed by a Cary 500 UV–vis–NIR spectrophotometer at λ = 553 or 585 nm, respectively.

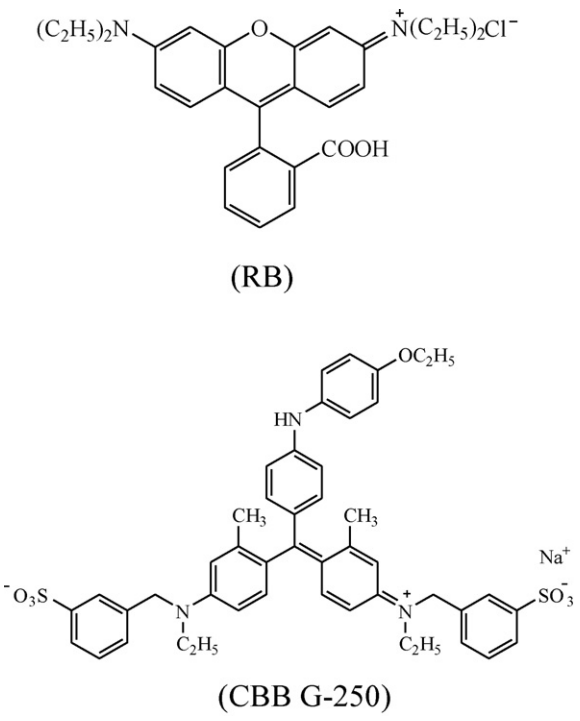

Scheme 1. Chemical structures of RB and CBB.

2.3.2. Degradation of dyes under UV-light irradiation

The light source is a high-pressure mercury lamp (125 W) with a main emission wavelength of 313 nm and an average light intensity of 1.75 mW cm^{-2}. The catalytic process is similar to section 2.3.1 except for the amount of catalysts is 0.15 g. Changes of total organic carbon (TOC) in the reaction system were monitored using a Shimadzu TOC-500 Total Organic Carbon analysis system. The structures of RB and CBB are illustrated in Scheme 1.

3. Results and discussion

3.1. Catalyst preparation

One-step sol–gel co-condensation technique combining with solvothermal treatment was applied to prepare Ag/V–TiO_2 composites, and the preparation procedure included the following three steps. Firstly, owing to mixing NH_4VO_3 and $AgNO_3$ was performed in presence of HNO_3, the formed silver vanadate precipitation was immediately dissolved into Ag^+ ion and V^{5+} species [22]. After mixing the above transparent solution with TTIP/i-PrOH solution in the presence of P123 under vigorous stirring, a sol of (Ti, V)–O_2 species with a large number of surface hydroxyl groups because of the incomplete condensation was formed. Continuous stirring the above sol at room temperature led to a gel of (Ti, V)–O_2 species due to the evaporation of most of solvent. In this sol–gel step, Ag^+ was adsorbed on the surface of (Ti, V)–O_2 species. Secondly, the obtained gel was suffered from solvothermal treatment at 473 K with a heating rate of 2 K min^{-1} for the purposes of (i) forming the product with crystal rather than amorphous phase; (ii) reducing the product particle size; and (iii) well-distributing the product particles. Importantly, Ag^+ was reduced into metallic Ag and part of V^{5+} species were reduced into V^{4+} species via the reaction with i-PrOH under the solvothermal condition. Similar results have been reported by Rengaraj and Li's group [23] and our previous work [24]. Finally, the surfactant P123 was removed together with the improved product crystallinity by successive thermal treatment at 313 K (24 h), 333 K (12 h), 353 K (2 h), 373 K (2 h), 393 K (0.5 h), and 723 K (3 h).

3.2. Catalyst characterization

3.2.1. Evolution of surface species

The nature of the surface species of as-prepared composite is studied by XPS surface probe technique, and the chemical states of Ag, V, and Ti species in the Ag/V–TiO_2-(1.8, 4.9) composite were obtained by analyzing its XPS results (Fig. 1). Fig. 1a shows the XPS of Ag/V–TiO_2-(1.8, 4.9) composite in the Ag $3d_{5/2}$ and Ag $3d_{3/2}$ binding energy (BE) regions. The determined BE of Ag $3d_{5/2}$ and Ag $3d_{3/2}$ is 367.8 and 373.8 eV, respectively, and the spin energy separation is 6.0 eV. This is the characteristic of metallic silver (Ag^0), and the shift of BE value of Ag was not observed [25]. The result suggests Ag species is deposited on the surface of the product rather than incorporated into the TiO_2 lattice. This is due to mismatching of ionic radii between Ag^+ (1.22 Å) and Ti^{4+} (0.74 Å) [26], as a result, the silver particles preferentially choose to segregate around the TiO_2 grain boundaries. Fig. 1b shows the XPS of Ag/V–TiO_2-(1.8, 4.9) in the V $2p_{3/2}$ and V $2p_{1/2}$ BE regions. Owing to very close BE value of V^{5+} $2p_{3/2}$ (516.4–517.4 eV) and V^{4+} $2p_{3/2}$ (515.4–515.7 eV) [27], the peak found at 516.7 eV is mainly ascribed to the V^{5+} $2p_{3/2}$, but the contribution of V^{4+} $2p_{3/2}$ is not excluded completely. Furthermore, the two overlapped peaks with BE range of 522.0 to 525.0 eV also evidence the presence of V^{4+} species in the composite. These two peaks are relatively broad and asymmetrical, and the peak centered at 523.6 eV is originated from V^{4+} $2p_{1/2}$ species; and the other peak centered at 524.5 eV is assigned to V^{5+} $2p_{1/2}$ species [28]. In Fig. 1c, the two peaks centered at 458.5 and 464.3 eV are assigned to the Ti $2p_{3/2}$ and Ti $2p_{1/2}$ of TiO_2, respectively. The doublet peaks are due to the spin-orbit splitting of Ti 2p and separated by 5.8 eV with an intensity ratio of 2.4. The results suggest that TiO_2 in the product is mainly anatase phase [29]. The O 1 s XPS spectrum (Fig. 1d) shows a narrow peak with a BE of 529.6 eV and slight asymmetry, corresponding to bulk oxygen bonded on TiO_2 or vanadium oxide. A little shift of the BEs of Ti and O are attributed to the polarization effect due to the incorporation of both V and Ag species within TiO_2 matrix [30].

3.2.2. XRD analysis

The crystalline phase of Ag/V–TiO_2-(1.8, 4.9) codoped system before and after annealing was characterized by XRD measurements. For comparison, pure TiO_2 and single-doped systems [Ag/TiO_2-(1.8, 0) and V–TiO_2-(0, 4.8)] prepared under the analogous conditions were also tested. Fig. 2a displays the XRD patterns of as-prepared products before annealing at 723 K, and the results show that the materials exhibit imperfect anatase crystal phase together with few rutile phase regardless of doping other components. From XRD patterns of the products obtained after annealing at 723 K it can be seen that their crystallinity become more perfect accompanying with considerable amount of rutile phase appeared (Fig. 2b). Concretely, pure TiO_2 was the mixture of anatase and rutile: the peaks at 25.28° (1 0 1), 37.90° (0 0 4), 48.02° (2 0 0), and 62.83° (2 0 4) correspond to anatase phase structure (JCPDS 21-1272); and the peaks at 27.8° (1 1 0), 36.08° (1 0 1), and 54.32° (2 1 1) originate from rutile phase (JCPDS 86-0147). The estimated anatase crystallite size from the (1 0 1) peak using the Scherrer formula is 11.2 nm, and the determined anatase to rutile ratio is 49.4:50.6 (Table 1). As for the single-doped Ag/TiO_2-(1.8, 0) material, its anatase to rutile ratio decreases slightly (43.1:56.9). However, in the case of single-doped V–TiO_2-(0, 4.8) material, the anatase to rutile ratio increased obviously (92.1:7.90). The estimated anatase crystallite size is 8.4 and 9.7 nm for Ag/TiO_2-(1.8, 0) and V–TiO_2-(0, 4.8) material, respectively. For the codoped Ag/V–TiO_2-(1.8, 4.9) material, the anatase to rutile ratio increase again (73.8:26.2); and the estimated anatase crystallite size is 7.7 nm. Compared with pure TiO_2, anatase crystal sizes for both of the single-doped (Ag/TiO_2 or V–TiO_2) and codoped (Ag/V–TiO_2) samples decreased, implying that doping Ag

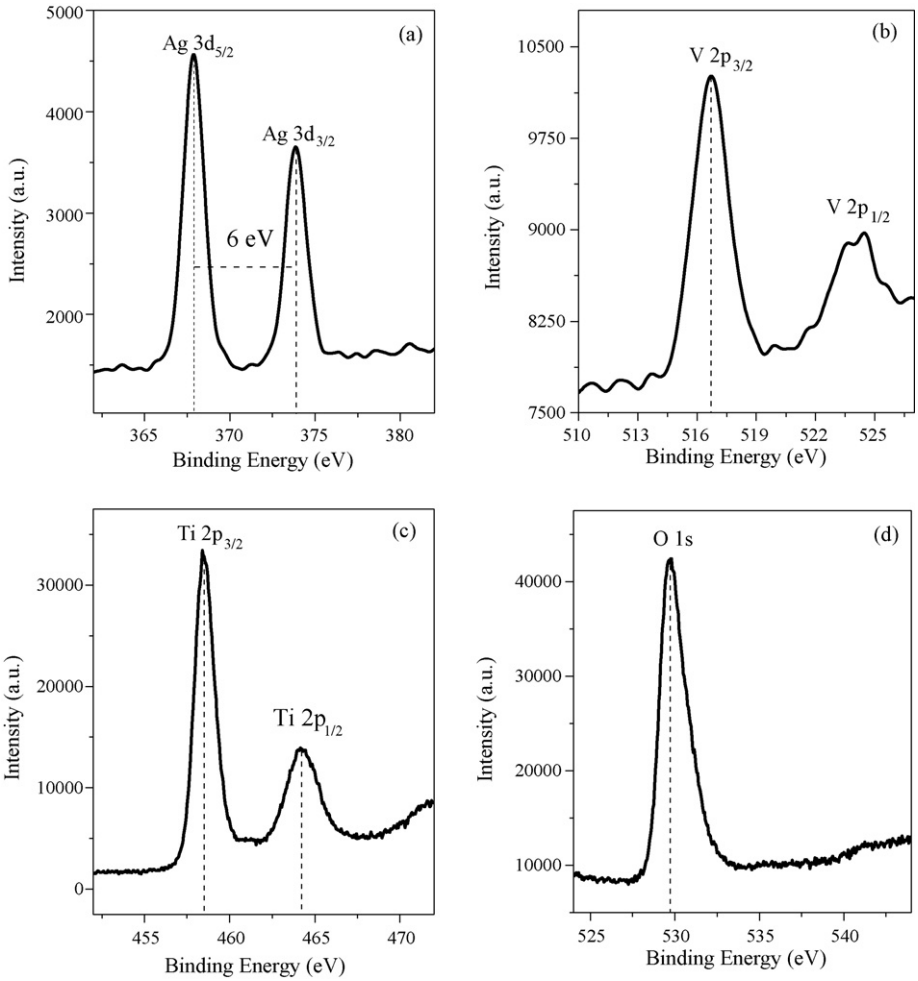

Fig. 1. XPS survey spectra for the Ag/V–TiO_2-(1.8, 4.9) nanocomposite in the (a) Ag 3d; (b) V 2p; (c) Ti 2p; and (d) O 1s binding energy regions.

or V within TiO_2 restrains the increase of grain size. The above results imply that: (i) higher annealing temperature (723 K) has a dominated influence on the phase structure and composition of as-prepared materials regardless of doping other components; and (ii) doping different components within TiO_2 results in the products with different phase structures and compositions. That is, doping vanadium oxide within TiO_2 can effectively hinder TiO_2 phase transformation from anatase to rutile; however, doping Ag only had a little effect on the TiO_2 phase transformation from anatase to rutile (Table 1). The results originated from the different doping modes of vanadium oxide and silver within TiO_2. From the above XPS results it is inferred that metallic Ag existed on the surface of the TiO_2 and vanadium cations entered into the TiO_2 crystal lattice. Consequently, influence of vanadium cations on the phase structures and compositions of the TiO_2 is more obvious compared with those of metallic Ag. Similar results have also been reported by other researchers. For examples, Fu and co-workers observed that doping Ag within TiO_2 promoted the anatase to rutile phase transformation, and they explained that there were two possible reasons for the decrease in the TiO_2 phase transformation temperature. One is that the density of surface defects would increase with the Ag doped, which would promote the phase transformation because the surface defects were considered as the rutile nucleation sites. The other is that the surface oxygen vacancy concentration of anatase grains is increased with the Ag doped, which favored the rearrangement of ions and reorganization of structure for rutile phase [31]. In the case of V-doped TiO_2, V^{4+} and/or V^{5+} ions that have replaced the Ti^{4+} sites will have a stabilizing effect on the Ti–O bond because the more electropositive V^{4+} and/or V^{5+} will render its electronic concentration to O^{2-} so that it can use this increased concentration of electrons to strengthen the bonding between the less electropositive Ti^{4+} ions. This stabilization of Ti–O bond will in turn retard the anatase-rutile transformation temperature because the anatase-rutile transformation needs the breakage of Ti–O bonds. Therefore,

Table 1
Summary of physicochemical properties of as-prepared samples.

Samples	Phase composition (%)		Crystalline size (nm)[a]	Lattice parameter (Å)		E_g (eV)
	Anatase	Rutile		*a*	*c*	
TiO_2	49.4	50.6	11.20	3.7794	9.4274	3.10
Ag/TiO_2-(1.8, 0)	43.1	56.9	8.39	3.7808	9.4570	2.78
V–TiO_2-(0, 4.8)	92.1	7.9	9.66	3.7860	9.5597	2.28
Ag/V–TiO_2-(1.8, 4.9)	73.8	26.2	7.69	3.7720	9.5977	2.25

[a] The average crystalline size of anatase in the samples.

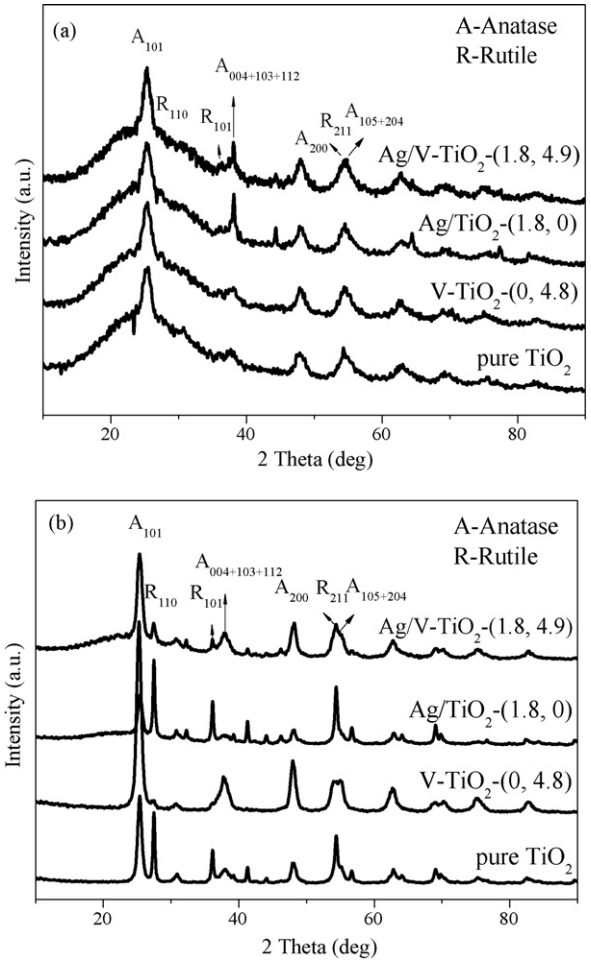

Fig. 2. XRD patterns of pure TiO_2; Ag/TiO_2-(1.8, 0); V–TiO_2-(0, 4.8); and Ag/V–TiO_2-(1.8, 4.9) before (a) and after (b) annealing at 723 K.

it is difficult to break the Ti–O bond because of the increased bond strength rendered by the V^{4+} and V^{5+} ions for the V-doped TiO_2. The role of vanadium doping was similar to that of La^{3+} ion doping within TiO_2 reported by Warrier's group [32]. Under the co-operation of vanadium oxide and Ag dopants, the Ag/V–TiO_2-(1.8, 4.9) codoped system exhibits the anatase to rutile ratio of 73.8:26.2. The value is similar to that of Degussa P25 (80:20), and it is lower than that of V–TiO_2-(0, 4.8) but higher than that of Ag/TiO_2-(1.8, 0).

In order to elucidate the nature of incorporation of Ag and V in the samples, the anatase peaks at 25.28° and 48.04° were used for calculating the unit cell parameters. From the calculated lattice parameters summarized in Table 1 it can be seen that the lattice parameters change little after Ag doping with respect to pure TiO_2, implying that Ag atoms existed on the surface of the composite rather than diffused into TiO_2 lattice. However, the lattice parameter of V–TiO_2-(0, 4.8) nanocomposites in the *c*-axis is larger than that of pure TiO_2, indicating a lattice expansion along the *c*-axis due to the incorporation of vanadium atoms. Therefore, it deduced that part of vanadium cations entered into the TiO_2 crystal lattice. Compared with V^{5+} ion (0.68 Å), the ion radii of six-coordinated V^{4+} (0.72 Å) is much closer to that of Ti^{4+} (0.74 Å) [33]. In addition, TiO_2 and VO_2 have a similar tetragonal crystal structure, whereas V_2O_5 has an orthorhombic or much distorted tetragonal pyramidal crystal structure. This fact implies that V^{4+} ions are easier to substitute for Ti^{4+} sites compared with V^{5+} ions. Similar result has also been found by other researchers [14,17,34]; additionally, subsequent UV–vis/DRS analysis result further confirms this conclusion

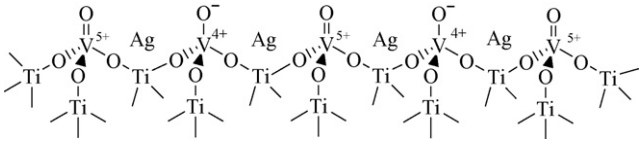

Scheme 2. Schematic representation of the Ag/V–TiO_2 composite.

(see Section 3.2.3). The diffraction peaks originated from the Ag is hardly detected in the Ag/V–TiO_2-(1.8, 4.9) composite. This may be due to the fact of homogeneous dispersion of Ag particles on the surface of the product.

Based on the above XPS and XRD discussion, schematic representation of the Ag/V–TiO_2 material is proposed (Scheme 2). In this material, part of V^{4+} or V^{5+} species enter into the TiO_2 crystal lattice due to the substitution for Ti^{4+} and form Ti−O–V bonds on the surface of the material; meanwhile, Ag particles disperse on the surface of the particles.

3.2.3. UV–vis/DRS analysis

It is well known that, in addition to the crystal structure, the electronic structure of a semiconductor material usually plays a dominant role in its photocatalytic activity. Bulk TiO_2 is a wide band gap semiconductor with a band gap energy of 3.2 eV (387 nm) for anatase and 3.0 eV (413 nm) for rutile [29]. The band gap energy is too large for TiO_2 to absorb visible light, therefore, the introduction of V species with different V loadings is expected to decrease band gap energy of TiO_2 in some extent.

Herein, the electronic structure of as-prepared materials was studied by their optical response though UV–vis/DRS determination. Fig. 3a shows the UV–vis/DRS of pure TiO_2, single (Ag or V) doped TiO_2, and co (Ag and V) doped TiO_2. Compared to the absorption spectrum of pure TiO_2, the absorption edge was shifted to the longer wavelength region in the spectra of all the doped TiO_2 materials. Calculated from the formulation of the maximum excited wavelength (λ_g) and band gap energy (E_g): λ_g (nm) = 1240/E_g (eV), the absorption threshold of pure TiO_2 is 400 nm, corresponding to the E_g of 3.1 eV (Table 1), attributed to charge transfer (CT) of O 2p orbitals to Ti 3d orbitals. The difference of E_g between as-prepared TiO_2 and TiO_2 with pure anatase phase is due to the existence of some rutile phase in as-prepared TiO_2. The electronic structure of TiO_2 can be tuned more or less through partial substitution of Ti^{4+} lattice sties by V^{5+} or V^{4+} ions. Such a modification in electronic structure may further affect its optical properties. As can be seen in Fig. 3a, V–TiO_2-(0, 4.8) sample exhibits absorption in the range of 200–600 nm and extends to 800 nm. It has been reported that V^{5+} shows absorption lower than 570 nm and that V^{4+} has an absorption band centered at 770 nm [35], therefore, the electron spectrum of V–TiO_2-(0, 4.8) suggests co-existence of V^{5+} and V^{4+} species in the composite, consistent with the XPS result. The tailing of the absorption band of V–TiO_2-(0, 4.8) can be assigned to the CT transition from the 3d orbitals of V^{4+} species to the Ti 3d orbitals of TiO_2 [36]. The calculated E_g of V–TiO_2-(0, 4.8) is 2.28 eV, and the result is closely related to the band structure of V–TiO_2-(0, 4.8). The CB of V–TiO_2-(0, 4.8) is mainly composed of the empty Ti 3d orbitals and some contributions from V^{5+} 3d and V^{4+} 3d orbitals. Form the UV–vis/DRS of V–TiO_2-(0, 4.8) it is inferred that the Ti 3d and V 3d orbitals are hybridized to form CBs of V–TiO_2. The conclusion is reasonable because: (i)

Table 2
Textural parameters of Ag/V–TiO_2 nanocomposites prepared with and without P123.

Samples	S_{BET} ($m^2\ g^{-1}$)	D_p (nm)	V_p ($cm^3\ g^{-1}$)
Ag/V–TiO_2-(1.8, 4.9)	96.7	12.4	0.35
P123-free-Ag/V–TiO_2-(1.9, 4.9)	67.2	12.8	0.25

no separated absorption peak originated from either TiO_2 or vanadium oxide appeared in the UV–vis/DRS of V–TiO_2-(0, 4.8); (ii) Ti 3d and V 3d orbitals possess very similar energy levels; and (iii) V^{5+}, V^{4+}, and Ti^{4+} species have similar ion radius. CT from O 2p orbitals to the hybridization orbitals (V^{5+} 3d + V^{4+} 3d + Ti^{4+} 3d) redshifts O 2p to Ti 3d CT band owing to lower energy level of the hybridization orbitals compared with Ti 3d orbitals. Consequently, band gap of V–TiO_2-(0, 4.8) is obviously decreased compared with pure TiO_2. As for single-doped Ag/TiO_2-(1.8, 0) sample, O 2p to Ti 3d CT band has somewhat redshift with E_g of 2.78 eV. This is because the metal clusters give rise to localized energy levels in the band gap of TiO_2 into which valence band electrons of TiO_2 are excited at wavelength longer than 400 nm [37]. Additionally, new absorption appears in the visible region (400–800 nm), attributed to the surface plasmon resonance of metallic silver nanoparticles, further substantiating the formation of Ag^0 in as-prepared composite [38]. In the case of codoped Ag/V–TiO_2-(1.8, 4.9) sample, its optical absorption response to UV- and visible-light is almost the same as that of single V species doped TiO_2 sample [V–TiO_2-(0, 4.8)] with E_g of 2.25 eV, implying that the deposition of Ag has little influence on the electronic structure of V–TiO_2-(0, 4.8) sample.

The influence of introduction of V into TiO_2 lattice on the optical absorption properties of pure TiO_2 is further studied (Fig. 3b). That is, an adsorption threshold shifts into the visible-light region even for the smallest vanadium content (0.9%). With increasing the amount of vanadium from 0.9 to 9.8%, there is a steady decrease in the E_g from 2.84 to 1.98 eV. The results suggest that E_g of a semiconductor could be tuned by incorporation of suitable metal ion with different loadings.

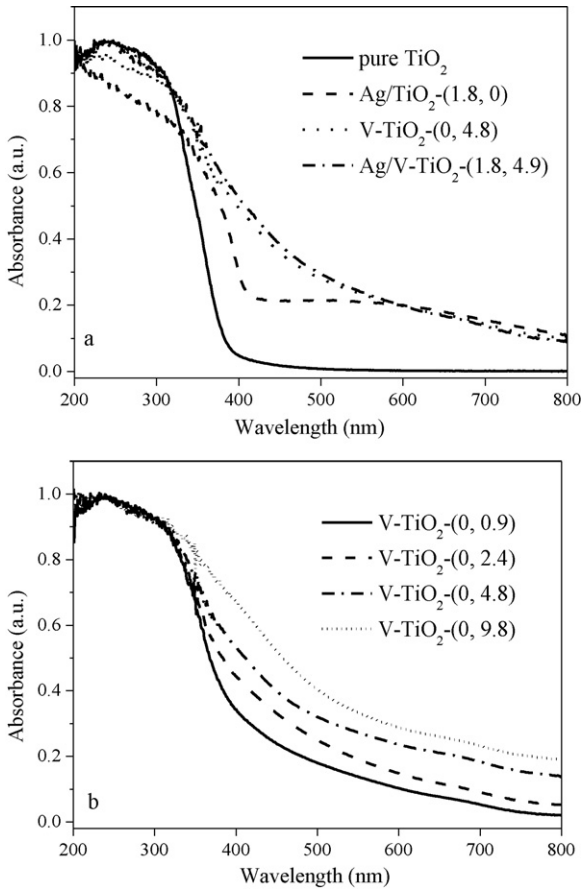

Fig. 3. UV–vis/DRS of (a) pure TiO_2; Ag/TiO_2-(1.8, 0); V–TiO_2-(0, 4.8); and Ag/V–TiO_2-(1.8, 4.9); and (b) V–TiO_2-(0, y) with y = 0.9, 2.4, 4.8, and 9.8%.

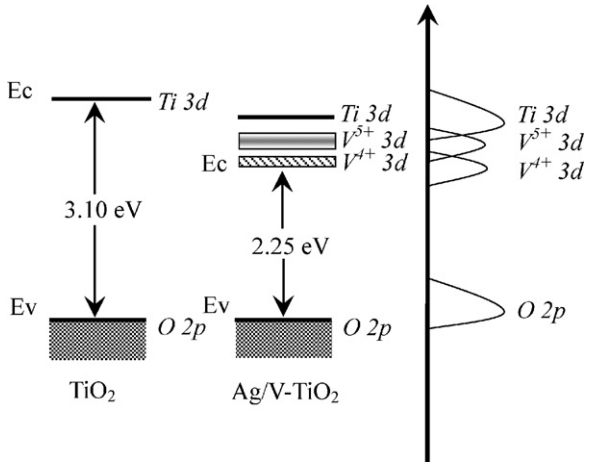

Fig. 4. Schematic band structure of pure TiO_2 and Ag/V–TiO_2.

Based on UV–vis/DRS results and the corresponding discussion, it confirms that the V doping can evidently narrow the band gap of TiO_2, and the proposed schematic band structure of pure TiO_2 and Ag/V–TiO_2 is shown in Fig. 4.

3.2.4. TEM images

TEM image of Ag/V–TiO_2-(1.8, 4.9) sample reveals the particle size is of ca. 12 nm, and a clear interface exists among the particles (Fig. 5a). The result suggests that the product particles pile up together loosely instead of aggregation. As for P123-free-Ag/V–TiO_2-(1.9, 4.9) sample (Fig. 5b), it shows obvious aggregation among particles with size of ca. 15 nm. The results suggest that P123 plays an important role to lead to well-dispersed nanocomposites with much smaller particle size. Similar results also have been reported for the preparation of highly dispersed and nanosized Ag/In_2O_3–TiO_2 composites [24]. The nanocomposites nature of Ag/V–TiO_2-(1.8, 4.9) is visibly observed in its high-resolution TEM images (Fig. 5c), showing the lattice fringes with an interlayer distance of 0.35 nm, extremely close to the lattice spacing of the (1 0 1) plane in anatase TiO_2.

3.2.5. Nitrogen adsorption–desorption

Fig. 6 shows nitrogen adsorption–desorption isotherms and pore size distribution curves of Ag/V–TiO_2 samples prepared with or without P123. Both of the isotherms exhibit Type IV with H3 hysteresis loop according to BDDT classification, which are typical characteristics of mesoporous materials [39]. Moreover, formation of such mesoporous material is attributed to the aggregation of the primary nanocomposites. The textural parameters including surface areas (S_{BET}), pore volumes (V_p), and median pore diameters (D_p) derived from the nitrogen adsorption–desorption isotherms are summarized in Table 2. It is found that the BET surface area of P123-free-Ag/V–TiO_2-(1.9, 4.9) sample is smaller than that of Ag/V–TiO_2-(1.8, 4.9) sample prepared in the presence of P123. This is due to the fact that the aggregation of the product particles was inhibited effectively due to the function of P123.

3.3. Photocatalytic activity

The photocatalytic activity of as-prepared pure TiO_2, single-doped TiO_2, codoped TiO_2, as well as the reference photocatalyst (Degussa P25) was tested via the degradation of dyes RB and CBB under visible- and UV-light irradiation. RB is a positively charged dye and CBB is an anionic dye. The reason for choosing dyes RB and CBB for current studies is to compare the different adsorption ability of two kinds of dyes over various as-prepared TiO_2-based

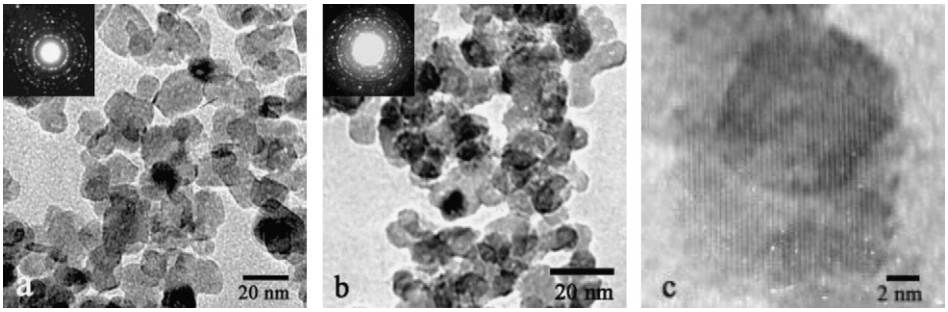

Fig. 5. TEM images of (a) Ag/V–TiO_2-(1.8, 4.9); (b) P123-free-Ag/V–TiO_2-(1.9, 4.9); and (c) high-resolution TEM image and the lattice fringe of Ag/V–TiO_2-(1.8, 4.9).

photocatalysts, and thereby to evaluate the influence of the dye adsorption on their photocatalytic performance. Under the adopted experimental conditions, the degradation of the selected dyes is significant only when the catalyst and the light irradiation were applied simultaneously.

3.3.1. Degradation of RB under visible-light irradiation

The adsorption behaviors of RB on various tested catalysts were studied since dye adsorption on the surface of the catalyst plays an important role to improve the activity of the catalyst. From the results shown in Fig. 7 it is found that after the powder samples were dispersed into the aqueous RB solution for 30 min in dark, decrease of RB concentrations occurred. The results originated from the adsorption of RB molecules on the surface of TiO_2-based powders. For the catalysts prepared in the presence of P123, their adsorption capacity to RB molecules is in the order of TiO_2 < Ag/TiO_2-(1.8, 0) < V–TiO_2-(0, 4.8) < Ag/V–TiO_2-(1.8, 4.9) (Fig. 7a). As for the P123-free catalysts, similar adsorption behaviors were obtained, but their absorption capacity to RB is lower compared with the samples prepared in the presence of P123. For example, the adsorption capacity of Ag/V–TiO_2-(1.8, 4.9) sample with and without P123 towards RB is 27.5 and 25.6%, respectively (Fig. 7a and b). This is due to larger BET surface area of Ag/V–TiO_2-(1.8, 4.9) sample prepared in the presence of P123 (Table 2). The above adsorption experiment indicates that Ag and vanadium oxide codoped TiO_2 composites showed the highest adsorption capacity to RB molecules regardless of adding P123.

From Fig. 7a it can be seen that conversion of RB reached to 36.1, 40.0, 54.2, and 63.4%, respectively, after visible-light irradiation of TiO_2, Ag/TiO_2-(1.8, 0), V–TiO_2-(0, 4.8), and Ag/V–TiO_2-(1.8, 4.9) for 240 min. The tested P123-free samples show similar results to the samples prepared in the presence of P123 (Fig. 7b), however, the P123-free samples are less active compared with samples prepared in the presence of P123, *e.g.*, conversion of RB reached to 50.2 and 63.4% after visible-light irradiation of P123-free-Ag/V–TiO_2-(1.9, 4.9) and Ag/V–TiO_2-(1.8, 4.9) for 240 min, respectively. The above photocatalytic testing results show the samples prepared in the presence of P123 and the Ag and vanadium oxide codoped TiO_2 material exhibited higher visible-light photocatalytic activity to RB degradation compared to the P123-free samples and single-doped TiO_2 material as well as pure TiO_2, respectively. Pure TiO_2 has no response to visible-light, and degradation of RB under visible-light irradiation of TiO_2 is due to the sensitization effect of RB [29]. Certainly, the degradation of RB over various doped TiO_2 materials under visible-light irradiation should not exclude the possibility of the sensitization effect of dye. Therefore, codoping Ag and vanadium oxide within TiO_2 as well as adding P123 for catalyst preparation significantly enhances the photocatalytic activity of TiO_2 toward RB degradation.

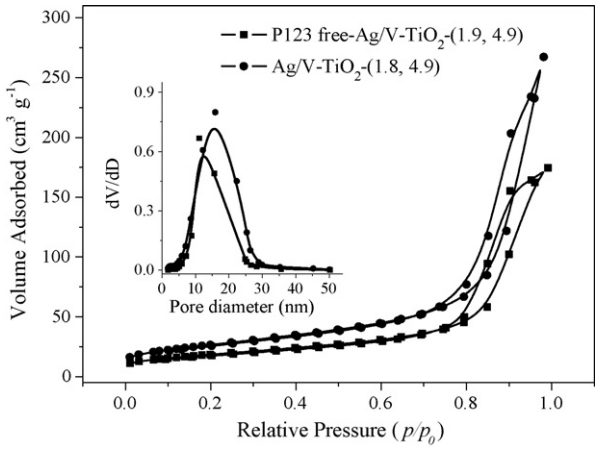

Fig. 6. Nitrogen adsorption–desorption isotherms and pore size distribution profiles (inset) according to BJH desorption d*V*/d*D* pore volume of Ag/V–TiO_2-(1.8, 4.9), and P123-free-Ag/V–TiO_2-(1.9, 4.9).

Influence of V dopings on the photocatalytic activity of V–TiO_2 materials was also studied. From Fig. 7c it can be seen that the photocatalytic activity of V–TiO_2 monotonically increased with the increase of V doping from 0.9 to 4.8%. However, further increasing V doping to 9.8% caused the decreased activity.

The photocatalytic activity of Ag/V–TiO_2 with varied amounts of Ag loading is shown in Fig. 7d. It can be seen that the photocatalytic activity of V–TiO_2-(0, 4.9) drastically increased after doping metallic Ag with lower levels (0.9–1.8%). Further increasing Ag loading to 4.9% lowered the activity.

3.3.2. Degradation of CBB under visible-light irradiation

Subsequently, degradation of dye CBB under visible-light irradiation of various TiO_2-based photocatalysts was studied. CBB was originally designed to be used as an acid wood dye, and it is an extremely popular reagent for protein chemists. The dye is used extensive for staining proteins in electrophoresis techniques, as well as for measuring protein concentration.

The adsorption behaviors of the tested TiO_2-based catalysts to CBB are different from those of RB. As can be seen from Fig. 8, TiO_2 and Degussa P25 showed the highest adsorption capacity to CBB, and they totally adsorbed CBB in the reaction system after stirring the suspension of an aqueous CBB and the catalyst for 30 min. As for the other tested materials, they displayed different adsorption capacities to CBB molecules: Ag/V–TiO_2-(1.8, 4.9) material showed stronger adsorption ability than that of V–TiO_2-(0, 4.8) or Ag/TiO_2-(1.8, 0) material. Adsorption of CBB molecules on the surface of TiO_2 or Degussa P25 is mainly due to the interaction existed between the positively charged surface ≡TiOH groups of TiO_2 and the negatively charged sulfonic acid groups of CBB molecule (Scheme 3). For the doped TiO_2 materials, considerable amount of surface ≡TiOH groups of TiO_2 were covered by the dopants (Ag and/or vanadium oxide), as a consequence, the adsorption ability of the doped TiO_2 materials to CBB became weaker obviously compared with pure

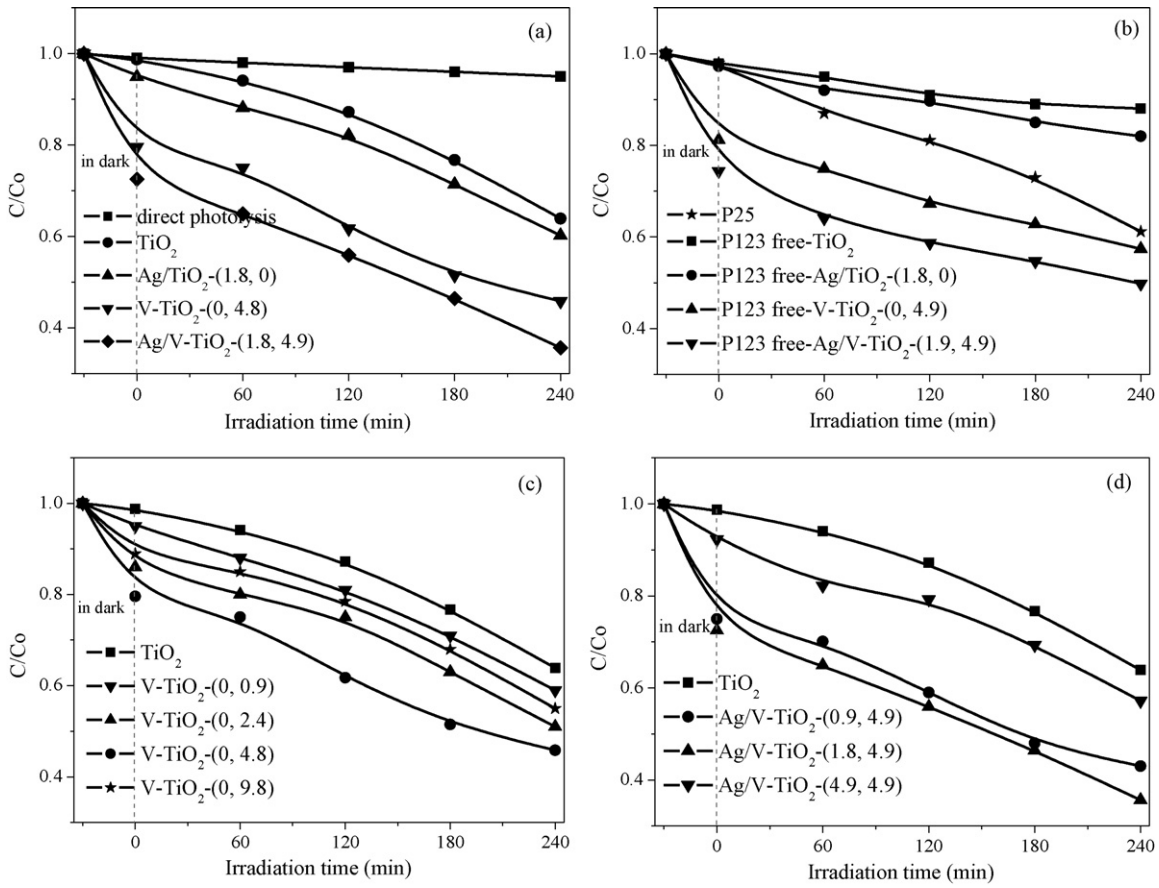

Fig. 7. Time courses of visible-light photodegradation of dye RB over (a) TiO_2-based samples prepared in the presence of P123; (b) Degussa P25 and P123-free-TiO_2-based samples; (c) V–TiO_2-(0, *y*) with *y* = 0.9, 2.4, 4.8, and 9.8%; and (d) Ag/V–TiO_2-(*x*, 4.9) with *x* = 0.9, 1.8, and 4.9%, respectively. C_0 and *C* is the original and residual RB concentration in the reaction system. C_0 of RB 25 mg L^{-1}. Catalyst 0.3 g.

TiO_2 or Degussa P25. Otherwise, RB is a positively charged dye, therefore, the adsorption ability of the doped TiO_2 materials to RB is much stronger compared with pure TiO_2.

Degradation of CBB reached to 64.9% after 240 min visible-light irradiation of Ag/V–TiO_2-(1.8, 4.9). Under the same conditions, degradation of CBB reached to 30.0 and 27.2%, respectively, by using V–TiO_2-(0, 4.8) and Ag/TiO_2-(1.8, 0). The results are similar to those obtained for RB degradation (see section 3.3.1).

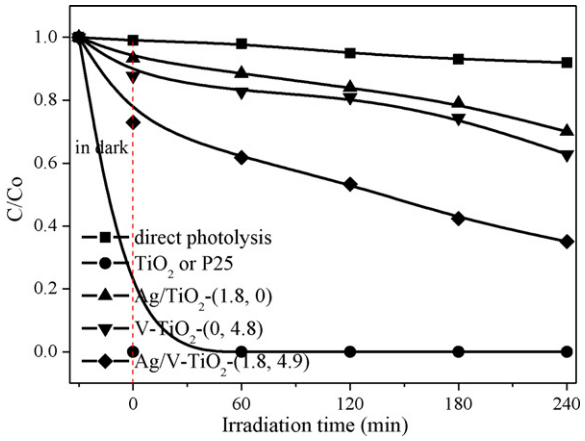

Fig. 8. Visible-light photodegradation of dye CBB over Degussa P25 and various TiO_2-based samples prepared in the presence of P123. C_0 and *C* is the original and residual CBB concentration in the reaction system. C_0 of CBB 25 mg L^{-1}. Catalyst 0.3 g.

3.3.3. Degradation and mineralization of RB or CBB under UV-light irradiation

The UV-light photocatalytic activity of codoped TiO_2 was studied by Ag/V–TiO_2-(1.8, 4.9). From the result displayed in Fig. 9a it is found that the material exhibited obviously high activity in current

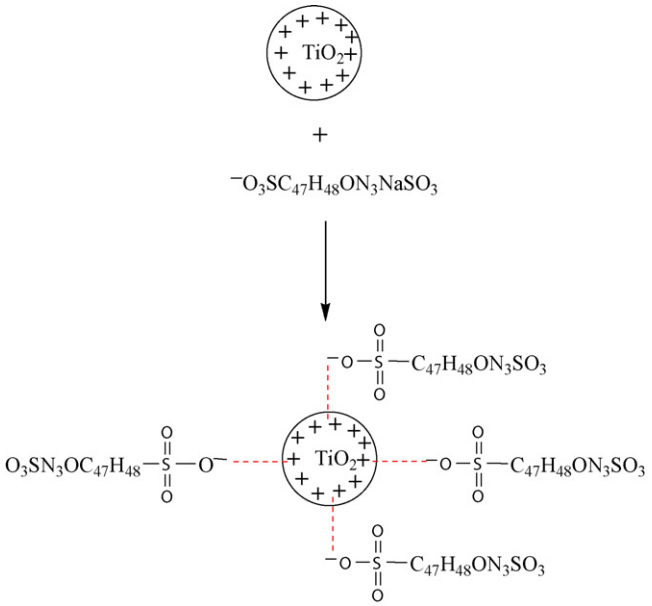

Scheme 3. How CBB is adsorbed on the TiO_2 or P25 surface.

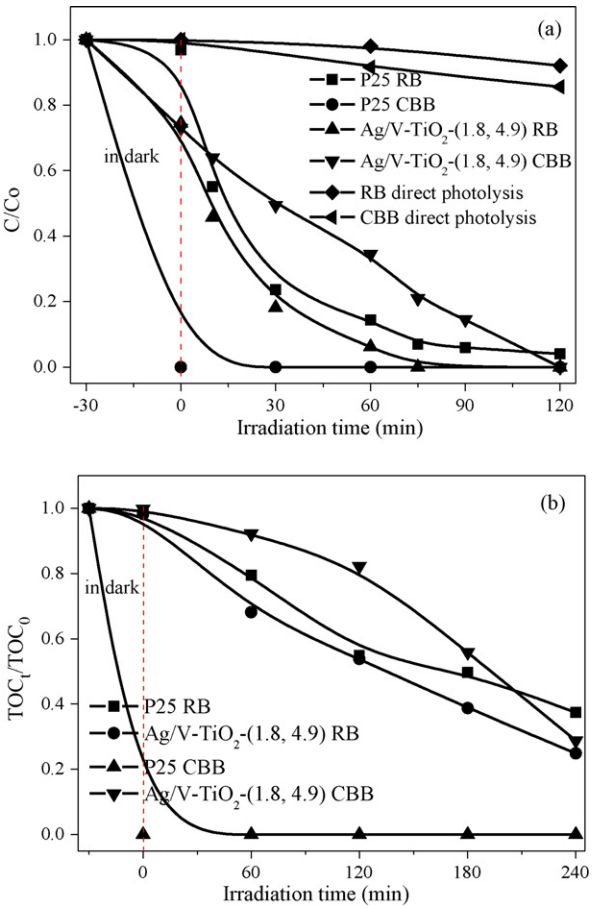

Fig. 9. Changes of concentration (a) and TOC (b) in the reaction systems during the process of UV-light photocatalytic degradation of dye CBB and RB over Degussa P25 and Ag/V–TiO_2-(1.8, 4.9) prepared in the presence of P123. C_0 of CBB or RB is 25 mg L^{-1}, respectively. Catalyst 0.15 g. TOC_0 and TOC_t is the original and residual CBB or RB total organic carbon in the reaction system.

photocatalytic system, and it took 75 and 120 min of UV-light irradiation to degrade RB and CBB totally. However, CBB was adsorbed on Degussa P25 completely.

It is a crucial step to mineralize dye during its photodecomposition process. In current reaction system, the mineralization ability of as-prepared Ag/V–TiO_2-(1.8, 4.9) nanocomposites to dye RB and CBB was evaluated by monitoring the changes of TOC (Fig. 9b). It is showed that after 240 min UV-light irradiation of Ag/V–TiO_2-(1.8, 4.9) and Degussa P25, the mineralization of RB reached to 75.2 and 62.6%, respectively. With the same UV-light irradiation time, the mineralization of CBB reached to 71.2% for Ag/V–TiO_2-(1.8, 4.9), but CBB still adsorbed on Degussa P25 totally.

3.3.4. Discussion

According to the above photocatalytic test results and the morphology, structure, and physicochemical properties of as-prepared Ag/V–TiO_2 three-component junction system, the excellent photocatalytic activity of the composite is attributed to the following reasons.

Firstly, the incorporation of vanadium ion into the crystal lattice of TiO_2 modifies the electronic properties of TiO_2, leading to the optical absorption of TiO_2 extend to the visible-light region. Therefore, the energy of the electron transition from the valence band to the conduction band is decreased, leading to more photogenerated carriers to participate in dye RB or CBB degradation reaction. However, the excessive vanadium species can also act as e^-–h^+ traps that may promote charge carrier recombination. As a consequence, V–TiO_2 with 9.8% V loading displayed lower photocatalytic activity than V–TiO_2 with 4.8% V loading towards RB degradation. Therefore, it is inferred that the band gap values of the photocatalytic materials are not the only reason to affect their photocatalytic activity.

Secondly, deposited metallic silver shows a positive influence on the photocatalytic activity of TiO_2 by facilitating e^-–h^+ pair separation since silver possesses strong electron trapping ability [24]. However, excessive silver doping led to the lower photocatalytic activity because part of TiO_2 surface was covered with excessive Ag particles, which may shield inner nanocomposites from light irradiation and affect the diffusion of the reactants. Alternatively, more than needed silver or vanadium doping may create the surface defect sites that may promote e^-–h^+ pair recombination and thereby decreasing the photoactivity [26].

Thirdly, a more important factor affecting the photocatalytic activity is the presence of anatase/rutile mixing phase in as-prepared TiO_2-based materials. The photocatalytic activity of these materials depends in part on the relative ratio of the two phases. Pure TiO_2 and Ag/TiO_2 exhibited low photocatalytic activity because of not-optimized anatase/rutile ratio (49.6:50.4 and 43.1:56.9). As for the Ag/V–TiO_2-(1.8, 4.9), the suitable ratio (73.8:26.2, similar to Degussa P25) is one of the factors to leading to its higher phtotcatalytic activity. In the mixed phase samples, h^+ and e^- were preferentially trapped on O^- and Ti^{3+} centers of the rutile phase, even when anatase is the main component. This indicates that electron transfer occurs from the higher energy CB states of anatase to those of rutile at lower energy and, simultaneously, h^+ transfer occurs from the lower energy valence band states of anatase to those of rutile at higher energy. This charge transfer is favored by the close contact between small anatase particles and larger rutile particles, and stabilizes the e^-–h^+ separation in the presence of rutile [40].

Finally, the surfactant P123 played an important role in the formation of well-distributed Ag/V–TiO_2 nanocomposites with larger BET surface area and larger adsorption capacity to the dye molecules. A good dispersion or reduced aggregation among Ag/V–TiO_2 particles may increase the active site-reactant contact opportunity and facilitate the electron transport. As for P123-free-Ag/V–TiO_2-(1.9, 4.9), its particle size is larger than that of the sample prepared with P123. Moreover, obvious aggregation and heterogeneous dispersion of Ag nanoparticles on the surface of V–TiO_2 occurred. Such bigger metal particles not only decrease the number of active sites for electron trapping but also enrich much more photogenerated electrons become new recombination centers of photogenerated carriers. In addition, smaller BET surface area of the P123-free sample also accounts for its lower photocatalytic activity.

4. Conclusions

The present work demonstrated a novel and simple route to prepare metallic silver and vanadium oxide codoped TiO_2 nanocomposites. At appropriate Ag and V dopings, the visible- and UV-light photocatalytic activity of the Ag/V–TiO_2 nanocomposites towards dyes RB and CBB degradation outperformed Degussa P25, as-prepared pure TiO_2, and single-doped Ag/TiO_2 or V–TiO_2 systems. The synergic contributions from the enhanced absorption in the visible-light region caused by doping vanadium oxide and the improved quantum efficiency due to doping metallic silver is the key factor in determining this enhanced photocatalytic activity; additionally, mixed phase structure with suitable anatase/rutile ratio of as-prepared Ag/V–TiO_2 also contributed to this enhanced photocatalytic activity. Except that, the surfactant P123 played an

important role in well dispersing Ag nanoparticles on the surface of the nanocomposites as well as enhancing the adsorption capacity to the dye molecules.

Acknowledgments

This work is supported by the Key Project of Chinese Ministry of Education (No. 308008); the Program for Changjiang Scholars and Innovative Research Team in University; The Natural Science Fund Council of China (20873018; 50878041; 50778036); and Analysis and Testing Foundation of Northeast Normal University.

References

[1] A.B. Santos, F.J. Cervantes, J.B. Lier, Review paper on current technologies for decolourisation of textile wastewaters: perspectives for anaerobic biotechnology, Bioresour. Technol. 98 (2007) 2369–2385.
[2] H. Lachheb, E. Puzenat, A. Houas, M. Ksibi, E. Elaloui, C. Guillard, J.M. Herrmann, Photocatalytic degradation of various types of dyes (alizarin S, crocein orange G, methyl red, congo red, methylene blue) in water by UV-irradiated titania, Appl. Catal. B: Environ. 39 (2002) 75–90.
[3] C.E. Bonancêa, G.M. Nascimento, M.L. Souza, M.L.A. Temperini, P. Corio, Substrate development for surface-enhanced Raman study of photocatalytic degradation processes: Congo red over silver modified titanium dioxide films, Appl. Catal. B: Environ. 69 (2006) 34–42.
[4] M.R. Hoffmann, S.T. Martin, W. Choi, D.W. Bahneman, Environment application of semiconductor photocatalysis, Chem. Rev. 1 (1995) 69–96.
[5] M. Anpo, M. Takeuchi, The design and development of highly reactive titanium oxide photocatalysts operating under visible light irradiation, J. Catal. 216 (2003) 505–516.
[6] T. Umebayashi, T. Yamaki, H. Itoh, K. Asai, Analysis of electronic structures of 3d transition metal-doped TiO_2 based on band calculations, J. Phys. Chem. Solids 63 (2002) 1909–1920.
[7] X. Chen, C. Burda, The electronic origin of the visible-light absorption properties of C-, N- and S-doped TiO_2 nanomaterials, J. Am. Chem. Soc. 130 (2008) 5018–5019.
[8] S. Usseglio, A. Damin, D. Scarano, S. Bordiga, A. Zecchina, C. Lamberti, $(I_2)_n$ encapsulation inside nanovoid-structured TiO_2: a way to tune the photoactivity in the visible region, J. Am. Chem. Soc. 129 (2007) 2822–2828.
[9] Z. Bian, J. Zhu, S. Wang, Y. Cao, X. Qian, H. Li, Self-assembly of active Bi_2O_3/TiO_2 visible photocatalyst with ordered mesoporous structure and highly crystallized anatase, J. Phys. Chem. C 112 (2008) 6258–6262.
[10] X. Chen, S.S. Mao, Titanium dioxide nanomaterials: synthesis, properties, modifications, and applications, Chem. Rev. 107 (2007) 2891–2959.
[11] H. Park, W. Choi, M.R. Hoffmann, Effects of the preparation method of the ternary $CdS/TiO_2/Pt$ hybrid photocatalysts on visible light-induced hydrogen production, J. Mater. Chem. 18 (2008) 2379–2385.
[12] L. Ge, M. Xu, H. Fang, Photo-catalytic degradation of methyl orange and formaldehyde by $Ag/InVO_4–TiO_2$ thin films under visible-light irradiation, J. Mol. Catal. A: Chem. 258 (2006) 68–76.
[13] M. Anpo, Preparation, characterization, and reactivities of highly functional titanium oxide-based photocatalysts able to operate under UV–visible light irradiation: approaches in realizing high efficiency in the use of visible light, Bull. Chem. Soc. Jpn. 77 (2004) 1427–1442.
[14] H. Yamashita, H. Harada, J. Misaka, M. Takeuchi, K. Ikeue, M. Anpo, Degradation of propanol diluted in water under visible light irradiation using metal ion-implanted titanium dioxide photocatalysts, J. Photochem. Photobiol. A 148 (2002) 257–261.
[15] J. Zhou, M. Takeuchi, A.K. Rayc, M. Anpo, X.S. Zhao, Enhancement of photocatalytic activity of P25 TiO_2 by vanadium-implantation under visible light irradiation, J. Colloid Interface Sci. 311 (2007) 497–501.
[16] M. Bettinelli, V. Dallacasa, D. Falcomer, P. Fornasiero, V. Gombac, T. Montini, L. Romanò, A. Speghini, Photocatalytic activity of TiO_2 doped with boron and vanadium, J. Hazard. Mater. 146 (2007) 529–534.
[17] A. Kubacka, A. Fuerte, A. Martínez-Arias, M. Fernández-Garcí, Nanosized Ti–V mixed oxides: effect of doping level in the photo-catalytic degradation of toluene using sunlight-type excitation, Appl. Catal. B: Environ. 74 (2007) 26–33.
[18] H. Chen, S. Chen, X. Quan, H. Yu, H. Zhao, Y. Zhang, Fabrication of TiO_2–Pt coaxial nanotube array Schottky structures for enhanced photocatalytic degradation of phenol in aqueous solution, J. Phys. Chem. C 112 (2008) 9285–9290.
[19] M.C. Hidalgo, M. Maicu, J.A. Navío, G. Colón, Effect of sulfate pretreatment on gold-modified TiO_2 for photocatalytic applications, J. Phys. Chem. C 113 (2009) 12840–12847.
[20] M.R. Mohammadi, D.J. Fray, A. Mohammad, Sol–gel nanostructured titanium dioxide: controlling the crystal structure, crystallite size, phase transformation, packing and ordering, Micropor, Mesopor. Mater. 112 (2008) 392–402.
[21] R. Spurr, H. Myers, Quantitative analysis of anatase–rutile mixtures with an X-ray diffractometer, Anal. Chem. 29 (1957) 760–762.
[22] J. Govaerts, C. Barcla-Goyanes, Radiochmical determination of chromium, vanadium and molybdenum by means of radioactive silver, Nature 168 (1951) 198.
[23] S Rengaraj, X.Z. Li, Enhanced photocatalytic activity of TiO_2 by doping with Ag for degradation of 2,4,6-trichlorophenol in aqueous suspension, J. Mol. Catal. A: Chem. 243 (2006) 60–67.
[24] X. Yang, Y. Wang, L. Xu, X. Yu, Y. Guo, Silver and indium oxide codoped TiO_2 nanocomposites with enhanced photocatalytic activity, J. Phys. Chem. C 112 (2008) 11481–11489.
[25] X. Wang, J.C. Yu, C. Ho, A.C. Mak, A robust three-dimensional mesoporous Ag/TiO_2 nanohybrid film, Chem. Commun. (2005) 2262–2264.
[26] R. Georgekutty, M.K. Seery, S.C. Pillai, A highly efficient Ag–ZnO photocatalyst: synthesis, properties, and mechanism, J. Phys. Chem. C 112 (2008) 13563–13570.
[27] B.M. Reddy, P.M. Sreekanth, E.P. Reddy, Surface characterization of La_2O_3-TiO_2 and V_2O_5/La_2O_3-TiO_2 catalysts, J. Phys. Chem. B 106 (2002) 5695–5700.
[28] C. Xu, L. Ma, X. Liu, W. Qiu, Z. Su, A novel reduction–hydrolysis method of preparing VO_2 nanopowders, Mater. Res. Bull. 39 (2004) 881–886.
[29] Y. Wang, Y. Wang, Y. Meng, H. Ding, Y. Shan, A highly efficient visible-light-activated photocatalyst based on bismuth- and sulfur-codoped TiO_2, J. Phys. Chem. C 112 (2008) 6620–6626.
[30] C. Su, C. Liao, J. Wang, C. Chiu, B. Chen, The adsorption and reactions of methyl iodide on powdered Ag/TiO_2, Catal. Today 97 (2004) 71–79.
[31] B. Xin, L. Jing, Z. Ren, B. Wang, H. Fu, Effects of simultaneously doped and deposited Ag on the photocatalytic activity and surface states of TiO_2, J. Phys. Chem. B 109 (2005) 2805–2809.
[32] C.P. Sibu, S.R. Kumar, P. Mukundan, K.G.K. Warrier, Structural modifications and associated properties of lanthanum oxide doped sol–gel nanosized titanium oxide, Chem. Mater. 14 (2002) 2876–2881.
[33] D. Gu, B. Yang, Y. Hu, V and N co-doped nanocrystal anatase TiO_2 photocatalysts with enhanced photocatalytic activity under visible light irradiation, Catal. Commun. 9 (2008) 1472–1476.
[34] M. Fernández-García, A. Martínez-Arias, J.C. Hanson, J.A. Rodríguez, Nanostructured oxides in chemistry: characterization and properties, Chem. Rev. 104 (2004) 4063–4104.
[35] H. Ozaki, S. Iwamoto, M. Inoue, Effect of the addition of a small amount of vanadium on the photocatalytic activities of N- and Si-co-doped titanias under visible-light irradiation, Catal. Lett. 113 (2007) 95–98.
[36] X. Yang, C. Cao, K. Hohn, L. Erickson, R. Maghirang, D. Hamal, K. Klabunde, Highly visible-light active C- and V-doped TiO_2 for degradation of acetaldehyde, J. Catal. 252 (2007) 296–302.
[37] N. Sobana, M. Muruganadham, M. Swaminathan, Nano-Ag particles doped TiO_2 for efficient photodegradation of direct azo dyes, J. Mol. Catal. A: Chem. 258 (2006) 124–132.
[38] T. Hirakawa, P.V. Kamat, Charge separation and catalytic activity of $Ag@TiO_2$ core-shell composite clusters under UV-irradiation, J. Am. Chem. Soc. 127 (2005) 3928–3934.
[39] J. Yu, H. Yu, B. Cheng, M. Zhou, X. Zhao, Enhanced photocatalytic activity of TiO_2 powder (P25) by hydrothermal treatment, J. Mol. Catal. A: Chem. 253 (2006) 112–118.
[40] R. Scotti, I.R. Bellobono, C. Canevali, C. Cannas, M. Catti, M. D'Arienzo, A. Musinu, S. Polizzi, M. Sommariva, A. Testino, F. Morazzoni, Sol–gel pure and mixed-phase titanium dioxide for photocatalytic purposes: relations between phase composition, catalytic activity, and charge-trapped sites, Chem. Mater. 20 (2008) 4051–4061.